Microscopic approach to NA and AA scattering in the framework of chiral effective field theory and Brueckner-Hartree-Fock theory

M. Toyokawa, M. Yahiro, T. Matsumoto, [A]K. Minomo, [A]K. Ogata, and [A]M. Kohno
Department of Physics, Kyushu University, Fukuoka, Japan
[A]Research Center for Nuclear Physics, Osaka University, Ibaraki, Japan

Abstract
We describe nucleon-nucleus (NA) and nucleus-nucleus (AA) elastic scattering based on the chiral two-nucleon forces (2NFs) and chiral three-nucleon forces (3NFs), using the standard microscopic framework composed of the Brueckner-Hartree-Fock method (BHF) and the g-matrix folding model. The g-matrix for symmetric nuclear matter is calculated from chiral 2NFs of N^3LO and chiral 3NF of N^2LO by using the BHF method. For elastic scattering, the optical potentials are calculated by folding chiral g-matrix with projectile and target density. This microscopic framework reproduces the experimental data with no adjustable parameter. Chiral-3NF effects are small for NA scattering, but sizable for AA scattering. Chiral 3NF, mainly originated from the 2π-exchange diagram, makes the folding potentials less attractive and more absorptive.

1. Introduction

One of the important issue in nuclear physics is to clarify the effects of three-nucleon force (3NF) on finite nuclei, nuclear matter, and nuclear reactions. Recently, a theoretical breakthrough on this issue was made with chiral effective field theory (Ch-EFT); see Refs. [1, 2] and references therein. Ch-EFT is a theory based on chiral perturbation theory and enables to determine two-nucleon force (2NF), 3NF, and many-nucleon forces systematically. The effects of chiral 3NF were analyzed in many papers, see Refs. [3, 4, 5] for some examples.

Another important issue in nuclear physics is microscopic understanding of the nucleon-nucleus (NA) and nucleus-nucleus (AA) scattering. Elastic scattering is the simplest process of the nuclear reaction, and it can be described with the optical potentials between two nuclei. Moreover the optical potentials are essential in describing not only elastic scattering but also inelastic scattering and transfer and breakup reactions.

The g-matrix folding model is the standard method for obtaining the optical potential microscopically. In this model, the potential is obtained by folding the g-matrix effective interaction with target density for NA scattering and with projectile and target densities for AA scattering. The g-matrix effective interaction is usually evaluated by Brückner-Hartree-Fock (BHF) method for positive energy with realistic 2NF and is obtained as density- and energy-dependent complex interaction [6, 7, 8].

In present work, we calculate the g matrix based on chiral 2NF and 3NF by the BHF method for positive energy, and apply the g matrix for NA and AA elastic scattering by using g-matrix folding model. The folding model with chiral g matrix well reproduce the experimental data for NA and AA scattering with no adjustable parameter. Therefore we can investigate chiral-3NF effects quantitatively on NA and AA elastic scattering with present framework. This work is summarized in Ref. [9].

2. Theoretical framework

2.1 g matrix calculation for 3NF

The g matrix for symmetric nuclear matter is evaluated from BHF method. The 3NF v_{123} is hard to treat in nuclear matter. We then derive an effective 2NF $v_{12(3)}$ from v_{123} by using mean field approximation [5], that is, v_{123} is averaged over the third nucleon in the Fermi sea:

$$\langle \boldsymbol{k}_1', \boldsymbol{k}_2' | v_{12(3)} | \boldsymbol{k}_1, \boldsymbol{k}_2 \rangle_A = \sum_{\boldsymbol{k}_3} \langle \boldsymbol{k}_1', \boldsymbol{k}_2', \boldsymbol{k}_3 | v_{12(3)} | \boldsymbol{k}_1, \boldsymbol{k}_2, \boldsymbol{k}_3 \rangle_A, \tag{1}$$

where the subscript A represents the antisymmetrization and the symbol $\boldsymbol{k}_i$ stands for quantum numbers, momentum and z component of spin and isospin, of the i-th nucleon. By using this approximation, the potential energy is evaluated as

$$\begin{aligned} &\frac{1}{2} \sum_{\boldsymbol{k}_1, \boldsymbol{k}_2} \langle \boldsymbol{k}_1, \boldsymbol{k}_2 | v_{12} | \boldsymbol{k}_1, \boldsymbol{k}_2 \rangle_A + \frac{1}{3!} \sum_{\boldsymbol{k}_1, \boldsymbol{k}_2, \boldsymbol{k}_3} \langle \boldsymbol{k}_1, \boldsymbol{k}_2, \boldsymbol{k}_3 | v_{123} | \boldsymbol{k}_1, \boldsymbol{k}_2, \boldsymbol{k}_3 \rangle_A \\ &\quad = \frac{1}{2} \sum_{\boldsymbol{k}_1, \boldsymbol{k}_2} \langle \boldsymbol{k}_1, \boldsymbol{k}_2 | v_{12} + \frac{1}{3} v_{12(3)} | \boldsymbol{k}_1, \boldsymbol{k}_2 \rangle_A. \end{aligned} \tag{2}$$

This means that the g matrix g_{12} should be calculated by

$$g_{12} \quad = \quad v_{12} + \frac{1}{3} v_{12(3)} + (v_{12} + \frac{1}{3} v_{12(3)}) G_0 g_{12} \tag{3}$$

with the nucleon propegator G_0 including the Q represents the Pauli exclusion operator. Here the single-particle energy $e_{\boldsymbol{k}}$ for a nucleon with momentum $\boldsymbol{k}$ in the denominator of G_0 is obtained by

$$e_{\boldsymbol{k}} = \langle \boldsymbol{k} | T | \boldsymbol{k} \rangle + \mathrm{Re}[\mathscr{U}(\boldsymbol{k})], \tag{4}$$

with the single-particle potential,

$$\mathscr{U}(\boldsymbol{k}) = \sum_{\boldsymbol{k}'}^{k_\mathrm{F}} \langle \boldsymbol{k}, \boldsymbol{k}' | g_{12} + \frac{1}{6} v_{12(3)} (1 + G_0 g_{12}) | \boldsymbol{k}, \boldsymbol{k}' \rangle_A, \tag{5}$$

where T is a kinetic-energy operator. See the ref [5] for detail of BHF calculation. In the present BHF calculation, the cutoff energy $\Lambda = 550$ MeV is used both for N^{3}LO 2NF and N^{2}LO 3NF. The low-energy constants of chiral nuclear forces are taken from Ref. [10] as $(c_1, c_3, c_4) = (-0.81, -3.4, 3.4)$ in units of GeV^{-1}, and the other constants $(c_D, c_E) = (-4.381, -1.126)$ are from Ref. [11].

Because the original chiral g matrix obtained from BHF calculation is numerical and nonlocal, it is inconvenient for many applications such as g-matrix folding model. The original chiral g matrix is localized by following the Melbourne group procedure [12, 13]. The localized g matrix is equivalent with the on-shell and near-on-shell matrix elements of the original g matrix. In the present work, we adopt three-range Gaussian form as the local g matrix for each of central, spin-orbit, and tensor components and for each spin-isospin channel

$$g^{ST}(s, \rho, E) = \sum_{i=1}^{3} g_0^{ST}(\rho, E) e^{s^2/\lambda_i^2}, \tag{6}$$

where λ_i is the range parameter and $g_0^{ST}(\rho, E)$ is the complex strength parameter. Here ρ is the density of the nuclear matter and E is the incident energy of the nucleon. The range parameters and strength

parameters are determined so as to reproduce the on-shell and near-on-shell matrix elements of the original chiral g matrix. We obtain the range parameters as $(0.4, 0.9, 2.5)$ for central component and (0.5,0.9,1.8) for spin-orbit and tensor components to minimize the χ^2-values of the matrix elements.

2.2 folding model

The NA and AA elastic scattering can be described by the one-body Schrödinger equation,

$$[T_{\boldsymbol{R}} + U - E]\,\chi = 0, \tag{7}$$

with the optical potential $U(\boldsymbol{R})$, where E is the incident energy of the projectile and $T_{\boldsymbol{R}}$ is the kinetic-energy operator concerning the relative coordinate $\boldsymbol{R}$ between the projectile and the target. The optical potential U is composed of the central (CE) and spin-orbit (LS), and the Coulomb (Coul) component,

$$U = U_{\rm CE} + U_{\rm LS}\boldsymbol{L}\cdot\boldsymbol{\sigma} + V_{\rm Coul} \tag{8}$$

The central and spin-orbit components of optical potential are calculated by single folding model for NA scattering and double folding model for AA scattering. The folding potentials contain the direct and knock-on exchange term $U^{\rm DR}$ and $U^{\rm EX}$. The knock-on exchange term is nonlocal, but the term can be localized with high accuracy by the Brieva-Rook approximation [6]. The validity of this approximation is shown in Refs. [14, 15]. The central component of the localized folding potential for NA scattering is written as

$$U^{\rm DR}_{\rm CE}(R) = \sum_{\mu'}\int d\boldsymbol{r}_{\rm T}\rho^{\mu'}_{\rm T}(r_{\rm T})g^{\rm DR}_{\mu\mu'}(s,\rho), \tag{9}$$

$$U^{\rm EX}_{CE}(R) = \sum_{\mu'}\int d\boldsymbol{r}_{\rm T}\rho^{\mu'}_{\rm T}(|\boldsymbol{r}_{\rm T}-\boldsymbol{s}/2|)\frac{3j_1(k_{\rm F}s)}{k_{\rm F}s}g^{\rm EX}_{\mu\mu'}(s,\rho)j_0(K(R)s), \tag{10}$$

where μ is the z component of the isospin, $\boldsymbol{r}_{\rm T}$ stands for the coordinate of the interacting nucleon from the center of mass of target, $\boldsymbol{s} = \boldsymbol{R} - \boldsymbol{r}_{\rm T}$. $\rho^{\mu'}_{\rm T}$ is the proton and neutron density of the target nucleus. $g^{\rm DR(EX)}_{\mu\mu'}$ is the direct (knock-on exchange) component of the effective interaction between two nucleons which is described by the combination of g^{ST}. Here, $K(R)$ is the local momentum defined as $\hbar K(R) \equiv \sqrt{2\mu(E - U_{\rm CE} - V_{\rm Coul})}$, and $K(R)$ is obtained self-consistently. For spin-orbit component of the folding potential and detail of the single folding model, see Ref. [16].

For AA scattering, the central component of the localized folding potential is written as

$$U^{\rm DR}_{\rm CE}(\boldsymbol{R}) = \sum_{\mu\mu'}\int d\boldsymbol{r}_{\rm P}\boldsymbol{r}_{\rm T}\rho^{\mu}_{\rm P}(r_{\rm P})\rho^{\mu'}_{\rm T}(r_{\rm T})g^{DR}_{\mu\mu'}(s',\rho), \tag{11}$$

$$U^{\rm EX}_{\rm CE}(\boldsymbol{R}) = \sum_{\mu\mu'}\int d\boldsymbol{r}_{\rm P}d\boldsymbol{r}_{\rm T}\rho^{\mu}_{\rm P}(|\boldsymbol{r}_{\rm P}-\boldsymbol{s}'/2|)\frac{3j_1(k^{\rm P}_{\rm F}s')}{k^{\rm P}_{\rm F}s'}\rho^{\mu'}_{\rm T}(|\boldsymbol{r}_{\rm T}+\boldsymbol{s}'/2|)\frac{3j_1(k^{\rm T}_{\rm F}s')}{k^{\rm T}_{\rm F}s'} \times g^{\rm EX}_{\mu\mu'}(s',\rho)j_0(K(R)s'/M), \tag{12}$$

where $\boldsymbol{r}_{\rm P}$ stands for the coordinate of the interacting nucleon from the center of mass of projectile, $\boldsymbol{s}' = \boldsymbol{r}_{\rm P} - \boldsymbol{r}_{\rm T} + \boldsymbol{R}$, and M is defined by the mass number of projectile and target nuclei $A_{\rm P}$ and $A_{\rm T}$ as $M = A_{\rm P}A_{\rm T}/(A_{\rm P}+A_{\rm T})$. See Refs. [17, 18] for the detail of the double folding model and the treatment of the local density ρ.

For the ^{4}He density, we use the phenomenological proton-density determined from electron scattering [19] in which the finite-size effect due to the proton charge is unfolded in the standard manner

[20]. The neutron density is assumed to have the same geometry as the proton one. For the target density, we take the matter densities calculated by the spherical Hartree-Fock method with the Gogny-D1S interaction [21] in which the spurious center-of-mass motion is removed in the standard manner [22].

3. Results

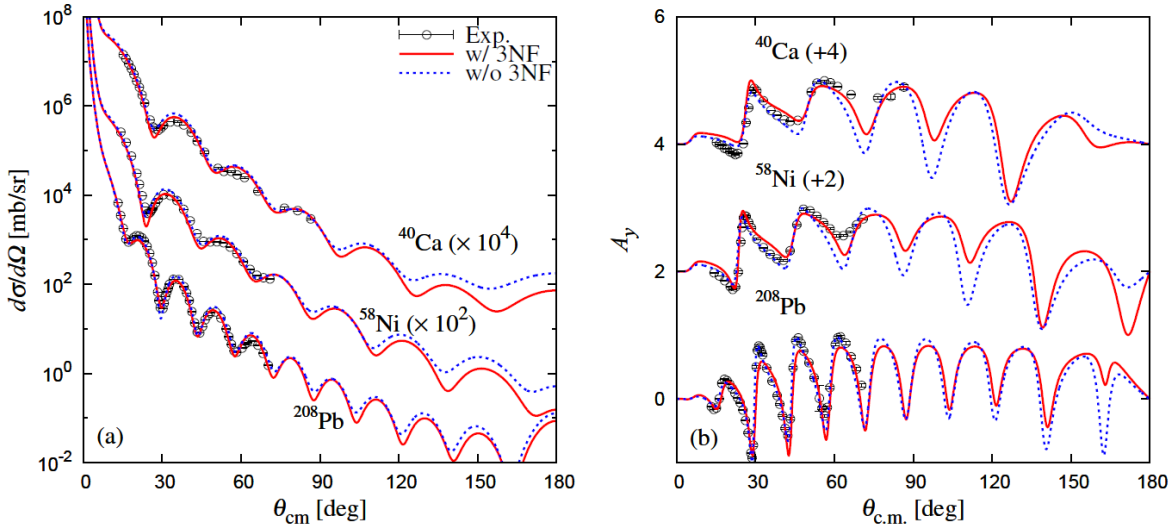

Fig. 1: The angular distribution of (a) differential cross sections and (b) vector analyzing powers for proton elastic scattering at $E = 65$ MeV. The solid and dashed lines represent to the results of chiral g matrix with and without 3NF effects, respectively. Each cross section is multiplied by the factor shown in the figure, while each vector analyzing power is shifted up by the number shown in the figure. Experimental data are taken from Ref. [23].

First, we consider proton elastic scattering at $E = 65$ MeV from ^{40}Ca, ^{58}Ni, and ^{208}Pb targets. Figure 1 shows the differential cross sections $d\sigma/d\Omega$ and vector analyzing power A_y as a function of scattering angle $\theta_{\rm c.m.}$. The solid and dashed lines represent the results of chiral g matrix with and without 3NF effects. One can see that the chiral g matrix well reproduce the experimental data [23] without any adjustable parameters. Chiral-3NF effects are small for $d\sigma/d\Omega$ at forward and middle angles where the data are available, because the scattering is governed by the potentials in the surface region where 3NF effects are small. However chiral-3NF effects for A_y are seen at middle angles $\theta_{\rm c.m.} \simeq 60^\circ$, because A_y is more sensitive for the difference of the potential than $d\sigma/d\Omega$.

Next, we show the results of ^{4}He elastic scattering at $E/A = 72$ MeV from ^{58}Ni and ^{208}Pb targets. Figure 2 show $d\sigma/d\Omega$ as a function of scattering angle $\theta_{\rm c.m.}$. The solid and dashed lines represent the results of chiral g matrix with and without 3NF effects. For both targets, chiral g matrix reproduce the experimental data [24] and chiral-3NF effects are sizable at middle angles $\theta_{\rm c.m.} > 20^\circ$. The reason why chiral-3NF effects are sizable for ^{4}He scattering can be explained by near-far decomposition [25]. When a detector is set on the right-hand side of the target, the outgoing wave going through the right-hand (left-hand) side of the target is called the near-side (far-side) scattering. The near-side (far-side) component is mainly induced by repulsive Coulomb (attractive nuclear) force, and in general the near-side (far-side) component dominates forward-angle (middle-angle) scattering. The oscillations of $d\sigma/d\Omega$, which are shown at $\theta_{\rm c.m.} = 5$–20° in Fig.2, are appeared because of the interference between the near- and far-side component. When the scattering is dominated by the far-side component, $d\sigma/d\Omega$ has no oscillation and is sensitive to the change of nuclear force. For ^{4}He scattering, the middle angle $\theta_{\rm c.m.} < 20^\circ$ is dominated by the far-side component and chiral 3NF effects appear in this region.

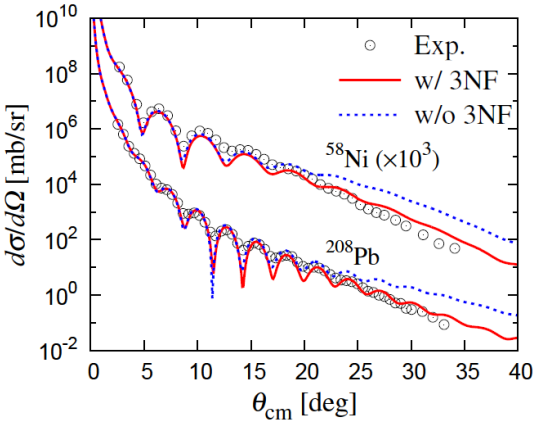

Fig. 2: The angular distribution of differential cross sections for ^{4}He elastic scattering at $E = 72$ MeV/nucleon from ^{5}8Ni and ^{208}Pb targets. The solid and dashed lines represent the results of the chiral g matrix with and without 3NF effects, respectively. Each cross section is multiplied by the factor shown in the figure. Experimental data are taken from Ref. [24]

Figure 3 shows the central part $U_{\rm CE}(R)$ of the folding potential for ^{4}He+^{208}Pb scattering at 72 MeV/nucleon. The solid and dashed lines represent the results of the chiral g matrix with and without 3NF effects. Chiral 3NF, mainly in its the 2π-exchange diagram, makes the potential less attractive and more absorptive. The repulsive effect mainly comes from the repulsion in the ^{1}E channel of g^{ST} because of the Pauli suppression of isobar Δ excitation in the nuclear-matter medium, and the absorptive effect mainly originated in the enhancement of the tensor correlations. The repulsive effect of chiral 3NF reduces $d\sigma/d\Omega$ at $\theta_{\rm c.m.} > 20^\circ$ for ^{4}He scattering, whereas stronger absorption from chiral 3NF better separates the far-side amplitude from the near-side one.

4. Summary

We described nucleon-nucleus (NA) scattering at 65 MeV and nucleus-nucleus (AA) scattering at 72 MeV/nucleon based on chiral two-nucleon forces (2NFs) and three-nucleon forces (3NFs), using the standard BHF method and the g-matrix folding model. We calculated the g matrix for the symmetric nuclear matter from N^{3}LO 2NF and N^{2}LO 3NF for positive energy by BHF method. Chiral-3NF effects are mainly come from the 2π-exchange diagram. Chiral 3NF in the ^{3}E channel enhances the tensor correlations and makes the optical potential more absorptive. In the ^{1}E channel, chiral-3NF effect make the optical potential less attractive because of the Pauli suppression of isobar Δ excitation in the nuclear-matter medium in the conventional picture.

We provided the chiral g matrix with a three-range Gaussian form by following the Melbourne-group procedure [12, 13]. The localization of the g matrix was performed by making a χ^2 fitting to the on-shell and near-on-shell matrix elements of the original chiral g matrix. This localized Gaussian g matrix makes the folding procedure much easier. The g-matrix folding model with the chiral g matrix well reproduced the experimental data with no adjustable parameter for proton and ^{4}He scattering from various target. We found that chiral-3NF effects are small for proton scattering but sizable for ^{4}He scattering at the middle angle $\theta_{\rm c.m.} > 20^\circ$. Chiral 3NF reduced the differential cross section at the middle angle because of its repulsive nature.

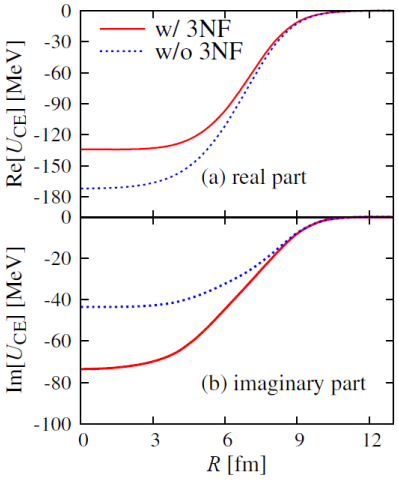

Fig. 3: R dependence of the central part of the folding potential for ^{4}He+^{208}Pb elastic scattering at $E = 72$ MeV/nucleon. The solid and dashed lines represent the results of chiral g matrix with and without 3NF effects. Panels (a) and (b) correspond to the real and imaginary parts of U_{CE}.

References

[1] E. Epelbaum, H. -W. Hammer, and Ulf-G. Meiσner, Rev. Mod. Phys. **81**, 1773 (2009).
[2] R. Machleidt and D. R. Entem, Phys. Rep. **503**, 1 (2011).
[3] N. Kalantar-Nayestanaki, E. Epelbaum, J. G. Messchendorp, and A. Nogga, Rep. Prog. Phys. **75**,016301 (2012).
[4] J. D. Holt, J. Menéndez, J. Simonis, and A. Schwenk, Phys. Rev. C **90**, 024312 (2014).
[5] M. Kohno, Phys. Rev. C **88**, 064005 (2013).
[6] F. A. Brieva and J. R. Rook, Nucl. Phys. A **291**, 299 (1977); **291**, 317 (1977); **297**, 206 (1978).
[7] K. Amos, P. J. Dortmans, H. V. von Geramb, S. Karataglidis, and J. Raynal, in *Advances in Nuclear Physics*, (Plenum, New York, 2000), Vol. 25, p. 275.
[8] T. Furumoto, Y. Sakuragi, and Y. Yamamoto, Phys. Rev. C **78**, 044610 (2008).
[9] M. Toyokawa, M. Yahiro, T. Matsumoto, K. Minomo, K. Ogata, and M. Kohno, Phys. Rev. C **92**, 024618 (2015).
[10] E. Epelbaum, W. Glöckle, and Ulf-G. Meiσner, Nucl. Phys. A **747**, 362 (2005).
[11] K. Hebeler, S. K. Bogner, R. J. Furnstahl, A. Nogga, and A.Schwenk, Phys. Rev. C **83**, 031301(R) (2011).
[12] H. V. von Geramb, K. Amos, L. Berge, S. Bräutigam, H. Kohlhoff, and A. Ingemarsson, Phys. Rev. C **44**, 73 (1991).
[13] P. J. Dortmans and K. Amos, Phys. Rev. C **49**, 1309 (1994).
[14] K. Hagino, T. Takehi, and N. Takigawa, Phys. Rev. C **74**, 037601 (2006).
[15] K. Minomo, K. Ogata, M. Kohno, Y. R. Shimizu, and M. Yahiro, J. Phys. G **37**, 085011 (2010).
[16] M. Toyokawa, K. Minomo, and M. Yahiro, Phys. Rev. C **88**, 054602 (2013).
[17] K. Egashira, K. Minomo, M. Toyokawa, T. Matsumoto, and M. Yahiro, Phys. Rev. C **89**, 064611 (2014).
[18] M. Toyokawa, T. Matsumoto, K. Minomo, and M. Yahiro, Phys. Rev. C **91**, 064610 (2015).
[19] H. de Vries, C. W. de Jager, and C. de Vries, At. Data Nucl. Data Tables **36**, 495 (1987).
[20] R. P. Singhal, M. W. S. Macauley, and P. K. A. De Witt Huberts, Nucl. Instrum. Methods **148**, 113 (1978).
[21] J. F. Berger, M. Girod, and D. Gogny, Comput. Phys. Commun. **63**, 365 (1991).
[22] T. Sumi *et al.*, Phys. Rev. C **85**, 064613 (2012).
[23] H. Sakaguchi *et al.*, Phys. Lett. B **89**, 40 (1979); **99**, 92 (1981).
[24] B. Bonin *et al.*, Nucl. Phys. A **445**, 381 (1985).
[25] R. C. Fuller, Phys. Rev. C **12**, 1561 (1975).